



Nanoscale

## Orientation and Morphology Control in Acid-Catalyzed Covalent Organic Framework Thin Films

Journal:	<i>Nanoscale</i>
Manuscript ID	NR-ART-11-2023-005798.R1
Article Type:	Paper
Date Submitted by the Author:	04-Feb-2024
Complete List of Authors:	<p>Bhagwandin, Dayanni; AFRL, RXESM; UES Inc, Division 30  Page, Kirt; Air Force Research Laboratory, Materials and Manufacturing  Tran, Ly; Air Force Research Laboratory  Yao, Yao; Northwestern University  Reidell, Alex; Air Force Research Laboratory, ;  Muratore, Christopher; University of Dayton, Department of Chemical  and Materials Engineering; Air Force Research Laboratory, Materials and  Manufacturing Directorate  Fang, Qiyi; Cornell University  Ruditskiy, Aleksey; Air Force Research Laboratory, Materials and  Manufacturing  Hampton, Cheri; AFRL, RXESM  Kennedy, William; Air Force Research Laboratory, Materials and  Manufacturing  Drummy, Lawrence; Air Force Research Laboratory Materials and  Manufacturing Directorate  Zhong, Yu; Cornell University  Marks, Tobin; Northwestern University, Chemistry  Facchetti, Antonio; Northwestern University, Department of Chemistry  and the Materials Research Center  Lou, Jun; Rice University, Department of Materials Science and  NanoEngineering  Koerner, Hilmar; Air Force Research Laboratory Materials and  Manufacturing Directorate, Composites Branch (RXCC)  Baldwin, Luke; Air Force Research Laboratory, Materials and  Manufacturing  Glavin, Nicholas; Air Force Research Laboratory, Materials and  Manufacturing</p>

# Orientation and Morphology Control in Acid-Catalyzed Covalent Organic Framework Thin Films

Dayanni D. Bhagwandin,<sup>a,b</sup> Kirt A. Page,<sup>a,b,c</sup> Ly D. Tran,<sup>a,b</sup> Yao Yao,<sup>d</sup> Alexander Reidell,<sup>a,b</sup> Christopher Muratore,<sup>e</sup> Qiyi Fang,<sup>f,g</sup> Aleksey Ruditskiy,<sup>a,b</sup> Cheri M. Hampton,<sup>a,b</sup> W. Joshua Kennedy,<sup>a</sup> Lawrence F. Drummy,<sup>a</sup> Yu Zhong,<sup>g</sup> Tobin J. Marks,<sup>d</sup> Antonio Facchetti,<sup>d,h</sup> Jun Lou,<sup>f</sup> Hilmar Koerner,<sup>a</sup> Luke A. Baldwin,<sup>a</sup> Nicholas R. Glavin<sup>†a</sup>

- 
- <sup>a</sup>. Materials and Manufacturing Directorate, Air Force Research Laboratory, Wright-Patterson Air Force Base, Ohio 45433, USA  
<sup>b</sup>. UES, Inc., Beavercreek, Ohio 45432, USA  
<sup>c</sup>. Cornell High Energy Synchrotron Source, Cornell University, Ithaca, New York 14853, USA  
<sup>d</sup>. Department of Chemistry and the Materials Research Center, Northwestern University, Sheridan Road, Evanston, IL 60208 USA  
<sup>e</sup>. Department of Chemical and Materials Engineering, University of Dayton, Dayton, Ohio 45469, USA  
<sup>f</sup>. Department of Materials Science and NanoEngineering, Rice University, Houston, Texas 77005, USA  
<sup>g</sup>. Department of Materials Science and Engineering, Cornell University, Ithaca, New York 14853, United States  
<sup>h</sup>. School of Materials Science and Engineering, Georgia Institute of Technology, Atlanta, Georgia 30332, USA

Keywords:

\*Corresponding author: Nicholas.Glavin.1@us.af.mil

## Abstract

As thin films of semiconducting covalent organic frameworks (COFs) are demonstrating utility for ambipolar electronics, channel materials in organic electrochemical transistors (OECTs), and broadband photodetectors, control and modulation of their thin film properties is paramount. In this work, a liquid-liquid growth technique is utilized to synthesize imine TAPB-PDA COF films at both the liquid-liquid interface as well as directly on a Si/SiO<sub>2</sub> substrate. The catalyst (acetic acid) concentration in the aqueous phase is shown to significantly influence direct growth thin film morphology, with concentrations below 1 M resulting in no film nucleation, concentrations

of 1-4 M enabling smooth film formation, and concentrations greater than 4 M resulting in films with a higher density of particulates on the surface. Importantly, while the films grown at the liquid-liquid interface are mixed-orientation, those grown directly on the Si/SiO<sub>2</sub> surface have highly oriented COF layers aligned parallel to the substrate surface. Moreover, the direct growth process affords TAPB-PDA COF thin films with p-type charge transport having a transconductance of 10  $\mu$ S at a gate voltage of -0.9V in an organic electrochemical transistor (OECT) device structure.

## Introduction

Covalent organic frameworks (COFs) are an extraordinarily versatile class of organic materials exhibiting nanoscale porosity, large-scale crystallographic ordering, and offering a vast library of prospective monomers and linker chemistries.<sup>1,2,3</sup> The synthesis of these materials is most commonly performed using solvothermal techniques to generate highly crystalline powders. However, in emergent applications requiring thin films, the fine control of thickness, morphology, crystallographic orientation, composition and structure is necessary to drive the desired properties of interest.<sup>4,5</sup> Current approaches towards growing high quality COF thin films directly onto solid substrates include bottom-up methods such as solvothermal synthesis,<sup>6,7,8,9,10,11,12,13,14,15,16,17,18,19,20,21,22,23</sup> vapor-assisted conversion,<sup>24</sup> continuous flow,<sup>25,26,27</sup> and interfacial synthesis. In the case of interfacial synthesis, the monomers are forced to react at liquid-liquid, liquid-solid, or liquid-air interfaces resulting in large grain sizes (micron-scale in some cases)<sup>28</sup> and some degree of controllable film thicknesses.<sup>29,30,31</sup> COF thin films synthesized using these methods typically result in films with varying degrees of crystallographic orientation on a wide variety of substrates.

In a typical liquid-liquid interfacial imine COF growth procedure, the reagents remain in separate immiscible phases in some cases featuring the acid catalyst in the aqueous phase separate from the amine and aldehyde monomers<sup>32</sup> while in others the amine monomer and acid catalyst are in the same phase.<sup>33</sup> These arrangements both force a majority of the COF thin film to form at the liquid-liquid interface where the highest concentration of all reagents meet. Recent work by Mahato et al.<sup>34</sup> reveals that films can be synthesized both at the interface and on a solid surface in the organic layer through residual crystallization in a liquid-liquid set up. In their work, a diamine linker which is placed in the top aqueous phase, reacts at the interface with trialdehyde linkers from the bottom organic phase to form a COF film. However, their work also demonstrates that the diamine linker is capable of diffusing into the organic layer and reacting with the trialdehyde near the surface of a substrate placed at the bottom. As a result, COF films can also form at this solid-liquid interface. Importantly, due to the slow diffusion of the monomers, the film formed at the solid-liquid interface exhibits a higher degree of crystallinity than the interfacially grown films.<sup>34</sup>

Here, we elaborate upon the liquid-solid growth technique to explore morphology and crystallographic orientation, two critical thin film properties for future applications, of imine COF films grown directly onto substrates (Figure 1a). We demonstrate that this residual/solid-liquid method (termed *direct growth* in this work) produces films with consistent thicknesses on the nanometer level which could be used for future electronic and optical device fabrication. This is in contrast to films grown at the liquid-liquid interface which produces micron level variations in thicknesses and can suffer from poor adhesion to some substrates. Additionally, we also show that the acid concentration strongly affects the morphology of the TAPB-PDA COF films with those most smooth achieved when the molarity of the acid in the aqueous phase is kept within a

certain range. Furthermore, we show that optimization of the growth time produces sub-20 nm films with nanometer level smoothness in just 30 minutes and illustrated that film orientation is strongly dependent upon growth conditions. These studies were culminated with a demonstration showing optimal films are semiconducting and function as the channel in organic electrochemical transistors.

## Results and Discussion

### COF Film Growth via Interfacial and Direct Growth

COF thin films were synthesized using the condensation reaction of 1,3,5-tris(4-aminophenyl) benzene (TAPB) (13 mg, 0.04 mmol, 1.0 eq) and *p*-phthalaldehyde (PDA) (7.5 mg, 0.06 mmol, 1.5 eq), which were added to a 20 mL scintillation vial and mixed with methylene chloride (8 mL) (Figure 1a). Next, a SiO<sub>2</sub>/Si substrate approximately 1 cm<sup>2</sup> was placed at the bottom of the vial. Then 8 mL of aqueous acetic acid (from 1 M to 10 M) was slowly syringed on top of the organic layer ensuring minimal disruption of the solvent-solvent interface. TAPB-PDA COF film (structure shown in Figure 1b) formation through interfacial growth (IG) and direct growth (DG) began almost instantly upon adding the aqueous layer containing the catalyst (shown in Figure 1c and d). After removing the substrate for DG, it was placed in a vial of acetone and briefly sonicated (<5 sec) to remove large particulates from the surface. Structural and chemical characterization of the TAPB-PDA COF grown both interfacially and directly on a substrate was carried out using Raman spectroscopy and Energy dispersive X-Ray spectroscopy (EDX). Figure 1e reports the Raman spectra of the monomer powders (PDA and TAPB) as well as the TAPB-PDA COF grown interfacially and directly on a substrate. The Raman peaks associated with the starting monomers were not present in the final COF thin films. Expected C=N stretching modes at 1590 and 1560 cm<sup>-1</sup> and aromatic stretching

modes for C-H at  $1160\text{ cm}^{-1}$  are instead present, indicating conversion of the monomer precursors to an imine network.<sup>35</sup> Additionally, the Raman spectra of the interfacial and direct growth TAPB-PDA COF both showed the same spectra with the exception of the  $\text{SiO}_2/\text{Si}$  substrate feature at  $520\text{ cm}^{-1}$  in the case of the thinner film from direct growth. EDX analysis was used to distinguish the film from the substrate. Areas containing the film had a higher percentage of carbon, while areas with only substrate had a higher percentage of silicon (further information in Figures S3 and S4).

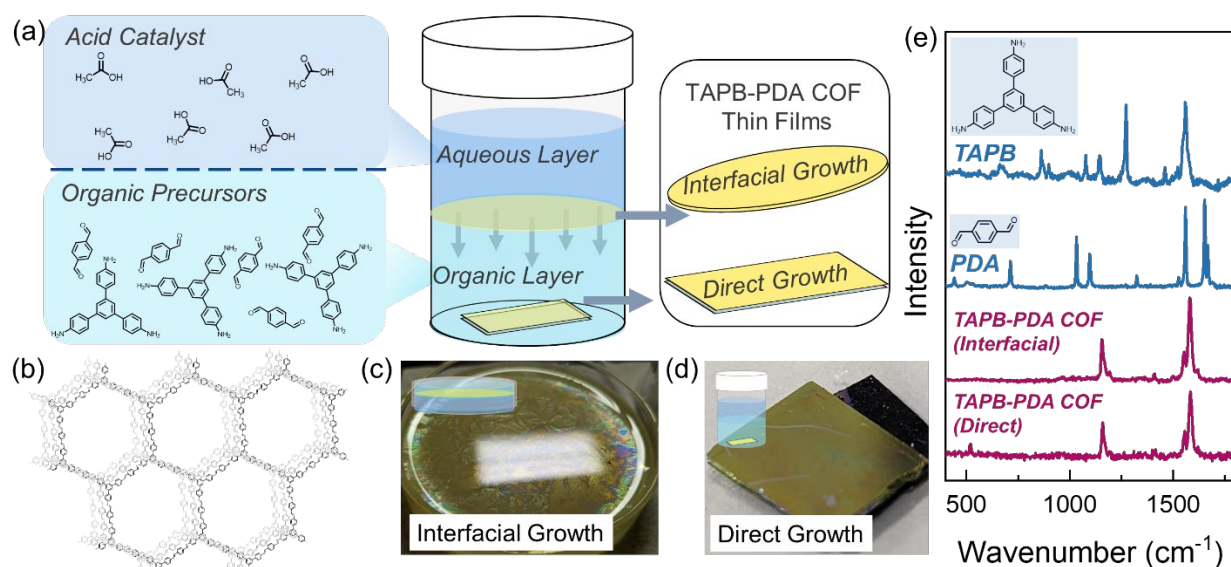


**Figure 1. Direct and Interfacial COF Growth.** (a) Interfacial and direct growth COF film setups; (b) Structure of TAPB-PDA COF; (c) Photograph of interfacial growth of COF film in petri dish; (d) photograph of direct growth of COF film on silicon substrate; (e) Raman spectra of precursors (TAPB and PDA) depicted in blue and TAPB-PDA COF film from interfacial and direct growth depicted in burgundy (silicon substrate peak at  $520\text{ cm}^{-1}$ ).

To fully characterize the TAPB-PDA COF (DG) and investigate the porosity, transmission electron microscopy (TEM) was conducted. An amorphous carbon coated TEM grid was attached to a silicon substrate and introduced to the direct growth setup. Afterwards, it was briefly sonicated to remove excess material and used for analysis. Figure 2 shows a close up real-space TEM image of the TAPB-PDA COF grown directly onto the TEM grid. The top right

corner of Figure 2 shows the corresponding fast Fourier transform (FFT) of the selected area indicating the periodicity originating from the [100] plane of the crystalline porous structure. It can clearly be noted that the pore size approaches 3.3 nm which closely matches previous literature reports of the same COF<sup>36</sup> (See Figures S5 and S6 in the supporting information for additional TEM images).

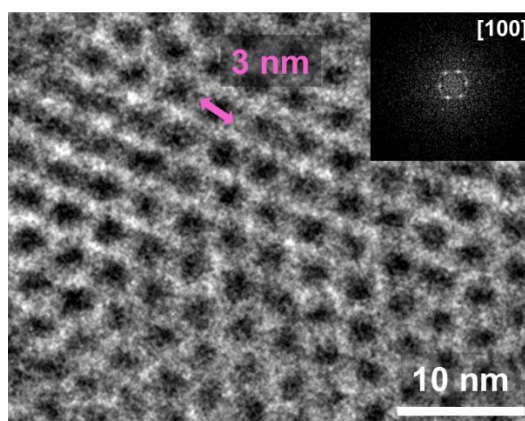


**Figure 2. TEM Image and Resulting FFT of TAPB-PDA COF (DG).** Pink arrow indicates pore distance of 3 nm and FFT shows the periodicity of the [100] plane arising from the porous crystalline structure.

### Acid Concentration Dependent Film Morphology in Direct Growth on Substrate

To study the effect of acid concentration on direct film growth, COF thin films were grown on Si/SiO<sub>2</sub> wafers using a range of molarities of acetic acid in the aqueous layer. Shown in Figure 3a, the higher concentration of acetic acid showed the visible presence of particulates in the bottom organic layer after 5 hours, while the lowest acid concentration showed minimal color change and absence of particulates in the organic solution (see additional Raman analysis in Figure S7 and time-lapse photographs in Figure S8 in the supporting information). To investigate the influence of acid molarity on film morphology, atomic force microscopy (AFM) was used to evaluate both surface roughness and film thickness (Figure 3b and c). Roughness analysis of the films grown both over 1 day and 7 days at varying acetic acid molarities reveals

that the acid concentration strongly affects the resultant surface roughness of the direct growth COF thin films (Figure 3b). AFM shows that acetic acid molarities below 1 resulted in very little nucleation or growth, as the catalyst concentration appears insufficiently high to initiate imine formation (Figure 3d). AFM also shows that with acid concentrations between 1 and 4 M, complete film formation with nanoscale roughness less than 4 nm is achieved, indicating ideal conditions for smooth and continuous TAPB-PDA COF film synthesis in this study (Figure 3e). Additional scanning electron microscopy (SEM) analysis is also included in Figure S9 in the supporting information. AFM shows that at higher acetic acid concentrations, the surface roughness dramatically increases as particulates ranging from 100-200 nm in area and approximately 15 nm in height form readily on the COF film (Figure 3f). Film thicknesses for experiments range between 150 – 200 nm with minimal difference between 1 day and 7 day growth, presumably due to the formation of an interfacial film between liquid-liquid interfaces.

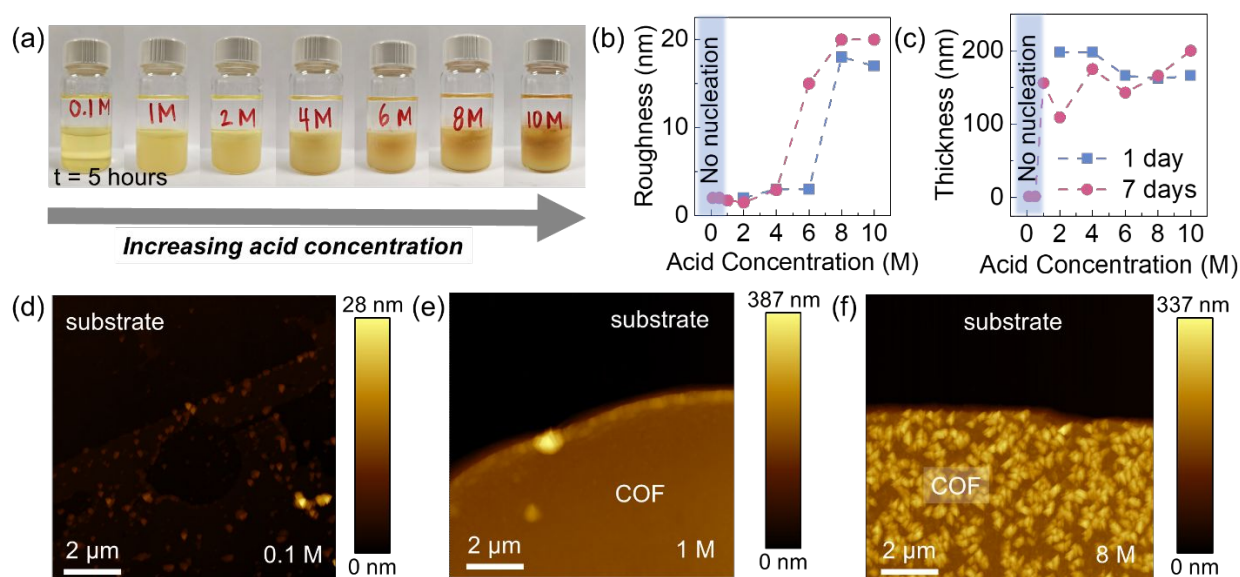


**Figure 3. Film Roughness and Thickness as a Function of Acid Concentration.** (a) Photographs exhibiting COF growth set up with range of different acid concentrations (0.1 M to 10 M AcOH) after 5 hours; (b) Graph of acid molarity and film roughness (nm); (c) Graph of acid molarity and film thickness (nm); (d) AFM of substrate after 7 days with 0.1 M AcOH



solution used in aqueous layer (no nucleation); (e) AFM of smooth COF thin film formed on substrate after 7 days with 2 molar AcOH solution used in aqueous layer (film thickness = 185 nm,  $R_q$  = 2 nm); (f) AFM of rough COF film formed on substrate after 1 day with 8 M AcOH solution used in aqueous layer (film thickness = 200 nm,  $R_q$  = 20 nm).

**Reaction Progression.** To further understand the growth reaction mechanism and progression, UV-Vis spectroscopy was used to explore the change in optical properties in the organic layer over time (see Figure 4a). To perform this experiment, an aliquot was removed from the middle of organic layer in the COF growth setup and diluted by 1,000x for analysis. The UV-Vis spectrum of the isolated monomers is shown in Figure 4a, which exhibits several unique peaks between 240 and 330 nm associated with both PDA and TABP in solution. Figure 4b shows the optical absorption spectrum of organic layer at various times with 2 M acetic acid in the aqueous layer, with evidence of the present monomers reducing substantially when approaching 24 hours. The rate of monomer consumption is strongly dependent upon the acid concentration,<sup>37</sup> as shown in Figure 4c with nearly all monomers consumed within 5 hours in the case of 8 M acetic acid concentration.

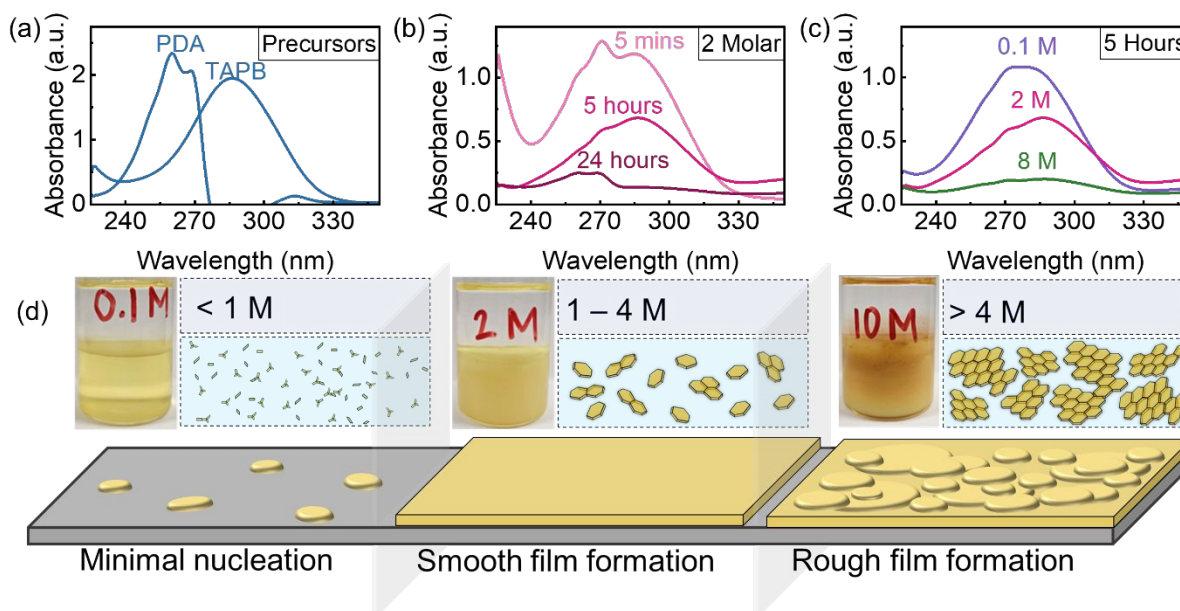


**Figure 4. Proposed Growth Mechanism of COF Film Under Different Acid Concentrations.** UV-Vis Absorption data for (a) Precursors PDA and TAPB, (b) Organic layer at 5 minutes, 5 hours, and 24 hours after reaction with 2 M acetic acid in aqueous layer (c) Organic layer after 5 hours with molarities of 0.1, 2, and 8; (d) Schematic of film formation as a result of acid concentration. Top left of each section shows photograph of reaction after 5 hours, top right of each section shows molarity range and resulting COF formation in organic layer.

The proposed thin film growth mechanism for acid-dependent growth of TAPB-PDA COF is shown in Figure 4d. For concentrations below 1 M, minimal film formation is observed, due to the limited concentration of COF oligomers present in solution and insufficient concentration of the acid to catalyze imine formation. However, when the acid concentration is between 1 M and 4 M, a generally smooth film is observed. This is due to the fact that sufficient acid has diffused across the interface enabling the reaction between the monomers, and thus driving the coalescence of crystalline domains. As a result, it is proposed that adequate, yet small-sized COF oligomers are present in the solution throughout and can therefore deposit and react onto the substrate. This produces accelerated COF growth in the lateral direction while limiting variations in thickness to less than 2 nm. Chen *et al.* describes a similar phenomenon of organic film growth where through Ostwald ripening, adjacent thin islands merge as a result of their high surface-to volume ratio and mobility on SiO<sub>2</sub>, leading to coalescence in the lateral direction. However, when the growing domain was isolated, it underwent a self-confined layer growth mode, leading to increase in the vertical direction.<sup>38</sup> The film morphology was found to be related to the percentage of molecules contained in islands greater than the critical island size, and thus justifies the observed film roughening shown in Figure 3f. When the acid concentration is greater than 4 M, a rough film is formed presumably due to a large presence of the acid catalyst that has diffused across the interface causing rapid uncontrolled imine bond formation between the monomers resulting large COF oligomers (Figure 4d, right). These oligomers deposit on the substrate surface and grow vertically to form a roughened film with large COF

clusters throughout and thus restricts smooth film formation in the lateral direction. Similarly, temperature related film roughening has been observed in vapor-solid COF growth via chemical vapor deposition (CVD).<sup>39</sup> Overall, film morphology and growth in the lateral versus vertical direction appears to be ultimately affected by the concentration of reacted monomers in solution.<sup>Error! Bookmark not defined.,40</sup>

**Time Dependent Film Morphology.** A major advantage to bottom-up COF growth using the techniques described herein is the ability to control film thickness. To probe if this method can be used to produce even thinner films, while retaining the overall smoothness, early direct growth film experiments were conducted. Figure 5a-f shows several AFM and SEM images of early-stage COF growth on Si/SiO<sub>2</sub> substrates. These results reveal that patchy COF film is deposited onto the substrate in as little as three minutes, as indicated by the AFM and SEM images shown in Figures 5a-b with cracks and uncoalesced film areas. At 30 minutes of growth time, smooth and continuous films can be observed which exhibit a more uniform film coverage with under 2 nm in film roughness throughout most parts (Figure 5c and d). After 100 minutes of growth time, a slight increase in roughness can be observed where Figure 5e-f shows occurrence of nanoscale islands/clusters on top of smooth film. It is evident that COF nucleation and film formation first takes place on the substrate through a nonclassical pathway,<sup>38</sup> and grows outwards until a smooth and continuous film is formed.<sup>41</sup> Afterwards, islands of COF begin to appear and extend upward,<sup>42</sup> justifying the Ostwald ripening mentioned previously. All COF films in this analysis appear under 60 nm in height. It should be noted however that early-stage growth does not produce wafer scale COF films and instead results in inhomogeneous growth throughout the substrate. Figure 5 summarizes the morphology of a majority of the COF film on the substrate but does not adequately define the entirety of the film. This is in comparison to the

growths lasting 24 hours or longer, which are capable of producing uniform and wafer scale films of greater thickness throughout. See Figures S10 – S15 in the Supporting Information for additional AFM and SEM images.

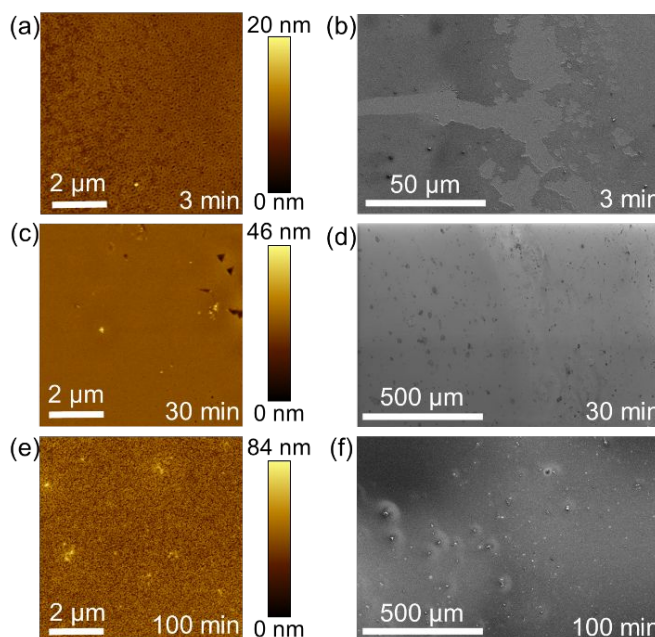


**Figure 5. Time Dependency and Early Film Formation.** (a) AFM image of uncoalesced film growth after 3 minutes (film thickness = 20 nm,  $R_q = 5$  nm); (b) SEM image of uncoalesced film after 3 minutes; (c) AFM image of coalesced smooth film after 30 minutes (film thickness = 37 nm,  $R_q < 2$  nm); (d) SEM image of coalesced film after 30 minutes; (e) AFM image of rougher film formation after 100 minutes (film thickness = 55 nm,  $R_q = 6$  nm); (f) SEM image of rougher film formation after 100 minutes

### Orientation Control

For future applications in electronic devices including sensors, ambipolar electronics, and transistor of different types, the control and manipulation of the COF film crystal orientation is critical. To study the influence of growth conditions on both the crystallinity and orientation of the TAPB-PDA COF thin films, grazing-incidence wide-angle X-ray scattering (GIWAXS) was performed. Prior to this analysis, the films underwent an annealing and subsequent activation step used to remove solvent and impurities from pores<sup>43</sup> (see further details in the Supporting

Information). The resulting scattering images and corresponding plots are shown in Figure 6. Several different films were analyzed (Figure 6a-d) ranging from direct growth to interfacial synthesis to understand the different effects of specific growth conditions. COF samples grown via direct growth on the substrate in both low and high acid concentration exhibit a high degree of crystallinity with COF layers aligned parallel to the substrate surface (Figure 6f, top). This level of crystallinity and orientation is retained even when the thickness of the COF film is increased after subjecting it to the same conditions again (Figure 6c). More information on this regrowth experiment can be found in Figures S16 and S17 in the Supporting Information. This preferred orientation is indicated by the vertical peaks that appear at between  $0.18 \text{ \AA}^{-1}$  and  $0.21 \text{ \AA}^{-1}$  in Figure 6a-d which correspond to the  $[100]$  of the hexagonal lattice.<sup>44,45,46</sup> Using Bragg's law, the d-spacing for these planes was determined from the peak position,  $q_{\max}$ , using the following equation:

$$d_{\text{Bragg}} = \frac{2\pi}{q_{\max}}$$

The d-spacings are  $32.2 \text{ \AA}$ ,  $32.4 \text{ \AA}$ ,  $32.2 \text{ \AA}$ , and  $33.2 \text{ \AA}$  for Figure 6 a-d, respectively which matches previous literature reports for the same COF.<sup>47, 48</sup> Additionally the PXRD data from the interfacially grown COF in Figure S1 was converted to I vs Q. The obtained pattern matches the 1D projection of the collected GIWAXS data from the direct growth film (see Figure S18 in the supporting information).

The parallel orientation of the COF relative to the surface of the substrate is a result of a few contributing factors of this unique direct growth setup. Firstly, the slow diffusion of the acetic acid across the interface controls the precise deposition and therefore lateral growth of the COF with initial preferential parallel orientation. Also, the interfacially formed COF between the

aqueous and organic layers likely plays a role in continuing to slow and control the acid diffusion. This is evident from the observed morphological features that occur when the acid concentration is changed as well as the early growth experiments depicted in the AFM images of Figures 3 and 5, respectively. Secondly, the preference for parallel orientation is retained as the COF film continues to grow in the vertical direction. This is likely due to the favorable  $\pi$ - $\pi$  interactions between the initial layers of COF and the layers that begin to form on top.<sup>49</sup> This has been previously observed in works which describe the growth of COFs on single-layer graphene (SLG) and show that the thickness and uniformity of orientated films are dependent on the underlying substrate.<sup>7,50</sup> This is also evident in Figure 6c, which shows that a COF film which was resubjected to the same growth conditions increases in thickness but retains parallel orientation.

Comparatively, the scattering image of the interfacial growth shown in Figure 6d depicts a circle with bright spots at the edges and top, suggesting randomly oriented crystallites (Figure 6f, bottom), similar to a powder.<sup>32</sup> The azimuthal integration for each scattering image is shown below in Figure 6. Figure 6e shows the scattering intensity versus  $\chi$  plots and distribution around the azimuth for COF samples in Figure 6a-d. All direct growth samples (Figure 6e; blue, pink, green) show a sharp decay in the azimuthal scattering from the 100 peak, indicating that the planes are vertically well-aligned with correlations in the direction parallel to the substrate surface. The interfacially grown sample (purple) is the outlier in this graph with a distribution of mixed orientations of the 100 planes relative to the substrate surface. This is likely due to the dynamic nature of the liquid-liquid interface, which aids in COF crystallization but does not cause any preferential alignment. Previous work has shown that a polymer is required to guide the ordering and alignment of COF crystallization at a liquid interface.<sup>28</sup>

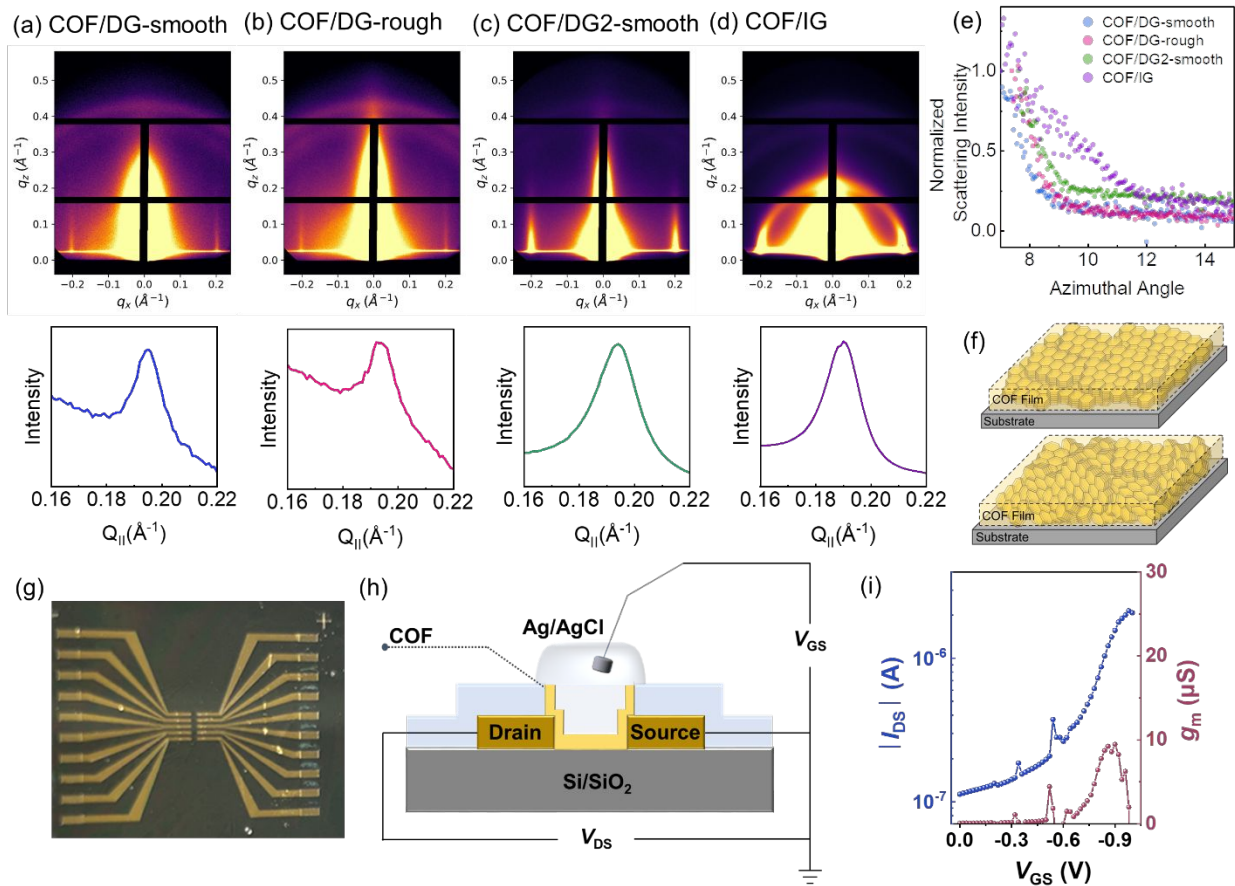


**Figure 6. Film Orientation with Grazing-Incidence Wide-Angle X-Ray Scattering and OCET performance.** (a-c) GIWAXS patterns and azimuthal integration for direct growth TAPB-PDA COF; (a) COF/DG-smooth (110 nm thickness), direct growth conditions: 2 molar, 7 days; (b) COF/DG-rough (160 nm), direct growth conditions: 8 M AcOH, 7 days; (c) COF/DG2-smooth, direct growth conditions: 1 M AcOH, 7 days, resubject to 1M AcOH, 3 days; (d) COF/IG, interfacial growth conditions: 0.1 M AcOH, 3 days in petri dish (e)  $I$  vs.  $\chi$  plot for a-d; (f) Parallel orientation (top) versus mixed orientation (bottom) schematic; (g) Photo image of transistor devices and (h) Schematic depiction of OCET device cross-section. (i) Transfer curve ( $V_{GS}$  from 0 V to  $-0.95$  V and  $V_{DS} = -0.7$  V) of a TAPB-PDA OCET with a  $W \times L$  of  $500 \mu\text{m} \times 10 \mu\text{m}$ .

### Semiconductor performance

Finally, we investigated TAPB-PDA COF films (DG) as the semiconductor channel in organic electrochemical transistors to access charge transport (Figure 6g). Organic electrochemical transistors operate by transducing a small gate voltage potential ( $V_{GS}$ ) into a channel current ( $I_{DS}$ )

between a source and drain electrodes.<sup>51,52</sup> The optical image of the OECTs array fabricated in this study is shown in Figure 6h while device fabrication process is shown in the Supporting Information (Figure S19). These OECTs have a channel dimension of  $500 \times 10 \mu\text{m}^2$  (width  $\times$  length) and details can be found in the Supporting Information. The transfer curve ( $I_{\text{DS}}-V_{\text{GS}}$ ) shown in Figure 6i indicates a p-type (hole transport) operation. These devices show typical gate modulation of the channel current over a gate voltage range from 0 V to  $-0.95$  V. The transconductance ( $g_{\text{m}}$ ), extracted from the slope of the transfer curve is a critical parameter for using an OECT as an amplifier. In this work, a maximum  $g_{\text{m}}$  of approximately  $9.5 \mu\text{S}$  at a gate voltage of  $-0.9$  V is measured. Note, the low current/transconductance values is expected considering the low semiconductor mass in the channel of these devices. Our TAPB-PDA COF films are quite thin ( $\sim 25$  nm) and have very low density ( $0.38 \text{ g/cm}^3$ )<sup>53</sup> compared to the typical conjugated organic polymers ( $\sim 100$  nm thick, density  $> 1 \text{ g/cm}^3$ ) commonly used in OECTs.<sup>54,55,56</sup> Additionally, the hydrophobic nature of the COF channel<sup>57</sup> may cause limited volumetric capacitance of electrochemical transistors operated in aqueous electrolyte. Future investigations of COF-based electrochemical transistors will focus on the optimization of COF film hydrophilicity,<sup>58</sup> which can be affected by crystallinity and surface area, and enhancement of the semiconducting monomer components.

## Conclusions

Ensuring strict control of crystallographic orientation and morphology during COF thin film growths remains a crucial parameter for implementation of these exciting materials into electronic and photonic applications. In this study, a liquid-liquid interfacial setup was used to synthesize COF thin films both at the interface and directly onto substrates at room temperature. The acetic acid concentration was found to strongly affect film morphology, where



concentrations 1 - 4 M enabled the formation of smooth films (<200 nm in thickness, 1-2 nm roughness) after 24 hours. Early growth experiments showed the evolution of film formation from patchy to smooth and uniform films and then to rougher and thicker films at longer growth times. GIWAXS studies highlight the difference in crystallinity between the direct growth and interfacial growth methods, where direct growth showed a high degree of parallel alignment to the substrate and interfacial growth showed mixed orientation. Finally, charge transport measurement of OECTs demonstrate that the present COF film are p-type semiconductor. In future applications utilizing transistors, optoelectronic devices, and catalytic films made from semiconducting COFs, understanding pore alignment and crystal structure in COF thin films will be important as electronic properties are governed by a multitude of factors. Future work linking thin film synthesis to controllable electronic properties of COFs will be important as the exciting materials continue to push the boundaries of wafer-scale organic electronic materials and potential device configurations.

### **Financial Support.**

D. D. B., L. T., L. B., and N. G. acknowledge financial support from The Air Force Office of Scientific Research (AFOSR) grant number 23RXCOR011. A. F. and T. J. M. gratefully acknowledge financial support by AFOSR grant FA9550-22-1-0423.

### **Author Contributions**

D. D. B., L. T., A. Re., Q. F., and C. M. performed COF synthesis and characterization. D. D. B., K. P., H. K. performed and evaluated GIWAXS experiments. A. Ru. performed SEM and surface characterization. C. H. performed TEM analysis. Y. Y. fabricated and evaluated OECT devices.

D. D. B., T. J. M., A. F., L. D., L. B., Y. Z., J. L., J. K. and N. G. led the supervision of experiments and manuscript preparation and drafting.

### **Conflicts of Interest**

There are no conflicts of interest.

### **Acknowledgements**

This material is based on research sponsored by AFRL under agreement number FA8650-22-2-5200. The U.S. Government is authorized to reproduce and distribute reprints for Governmental purposes notwithstanding any copyright notation thereon.

### **Notes and References**

## References

- 
- 1 A. P. Côté, A. I. Benin, N. W. Ockwig, M. O’Keeffe, A. J. Matzger and O. M. Yaghi, *Science*, 2005, **310**, 1166–1170.
  - 2 F. Haase and B. V. Lotsch, *Chem. Soc. Rev.*, 2020, **49**, 8469–8500.
  - 3 S. Kandambeth, K. Dey and R. Banerjee, *J. Am. Chem. Soc.*, 2019, **141**, 1807–1822.
  - 4 L. K. Beagle, Q. Fang, L. D. Tran, L. A. Baldwin, C. Muratore, J. Lou and N. R. Glavin, *Materials Today*, 2021, **51**, 427–448.
  - 5 J. L. Fenton, D. W. Burke, D. Qian, M. Olvera de la Cruz and W. R. Dichtel, *J. Am. Chem. Soc.*, 2021, **143**, 1466–1473.
  - 6 E. L. Spitler, B. T. Koo, J. L. Novotney, J. W. Colson, F. J. Uribe-Romo, G. D. Gutierrez, P. Clancy and W. R. Dichtel, *J. Am. Chem. Soc.*, 2011, **133**, 19416–19421.
  - 7 J. W. Colson, A. R. Woll, A. Mukherjee, M. P. Levendorf, E. L. Spitler, V. B. Shields, M. G. Spencer, J. Park and W. R. Dichtel, *Science*, 2011, **332**, 228–231.
  - 8 E. L. Spitler, J. W. Colson, F. J. Uribe-Romo, A. R. Woll, M. R. Giovino, A. Saldivar and W. R. Dichtel, *Angew. Chem. Int. Ed.*, 2012, **51**, 2623–2627.
  - 9 D. D. Medina, V. Werner, F. Auras, R. Tautz, M. Dogru, J. Schuster, S. Linke, M. Döblinger, J. Feldmann, P. Knochel and T. Bein, *ACS Nano*, 2014, **8**, 4042–4052.
  - 10 C. R. DeBlase, K. Hernández-Burgos, K. E. Silberstein, G. G. Rodríguez-Calero, R. P. Bisbey, H. D. Abruña and W. R. Dichtel, *ACS Nano*, 2015, **9**, 3178–3183.
  - 11 X. Gou, Q. Zhang, Y. Wu, Y. Zhao, X. Shi, X. Fan, L. Huang and G. Lu, *RSC Adv.*, 2016, **6**, 39198–39203.

- 
- 12 D. D. Medina, M. L. Petrus, A. N. Jumabekov, J. T. Margraf, S. Weinberger, J. M. Rotter, T. Clark and T. Bein, *ACS Nano*, 2017, **11**, 2706–2713.
- 13 L. D. Tran, B. J. Ree, A. Ruditskiy, L. K. Beagle, R. C. Selhorst, D. D. Bhagwandin, P. Miesle, L. F. Drummy, M. F. Durstock, R. Rao, H. Koerner, N. R. Glavin and L. A. Baldwin, *Adv. Mater. Interfaces*, 2023, **10**, 2300042.
- 14 L. Ascherl, E. W. Evans, M. Hennemann, D. Di Nuzzo, A. G. Hufnagel, M. Beetz, R. H. Friend, T. Clark, T. Bein and F. Auras, *Nat Commun*, 2018, **9**, 3802.
- 15 T. Sick, A. G. Hufnagel, J. Kampmann, I. Kondofersky, M. Calik, J. M. Rotter, A. Evans, M. Döblinger, S. Herbert, K. Peters, D. Böhm, P. Knochel, D. D. Medina, D. Fattakhova-Rohlfing and T. Bein, *J. Am. Chem. Soc.*, 2018, **140**, 2085–2092.
- 16 A. M. Evans, A. Giri, V. K. Sangwan, S. Xun, M. Bartnof, C. G. Torres-Castanedo, H. B. Balch, M. S. Rahn, N. P. Bradshaw, E. Vitaku, D. W. Burke, H. Li, M. J. Bedzyk, F. Wang, J.-L. Brédas, J. A. Malen, A. J. H. McGaughey, M. C. Hersam, W. R. Dichtel and P. E. Hopkins, *Nat. Mater.*, 2021, **20**, 1142–1148.
- 17 S. Cai, B. Sun, X. Li, Y. Yan, A. Navarro, A. Garzón-Ruiz, H. Mao, R. Chatterjee, J. Yano, C. Zhu, J. A. Reimer, S. Zheng, J. Fan, W. Zhang and Y. Liu, *ACS Appl. Mater. Interfaces*, 2020, **12**, 19054–19061.
- 18 Y. Chen, H. Cui, J. Zhang, K. Zhao, D. Ding, J. Guo, L. Li, Z. Tian and Z. Tang, *RSC Adv.*, 2015, **5**, 92573–92576.
- 19 S. Lin, C. S. Diercks, Y.-B. Zhang, N. Kornienko, E. M. Nichols, Y. Zhao, A. R. Paris, D. Kim, P. Yang, O. M. Yaghi and C. J. Chang, *Science*, 2015, **349**, 1208–1213.
- 20 L. Ascherl, E. W. Evans, J. Gorman, S. Orsborne, D. Bessinger, T. Bein, R. H. Friend and F. Auras, *J. Am. Chem. Soc.*, 2019, **141**, 15693–15699.
- 21 S. Jhulki, A. M. Evans, X.-L. Hao, M. W. Cooper, C. H. Feriante, J. Leisen, H. Li, D. Lam, M. C. Hersam, S. Barlow, J.-L. Brédas, W. R. Dichtel and S. R. Marder, *J. Am. Chem. Soc.*, 2020, **142**, 783–791.

- 
- 22 S. Zhang, Q. Yang, X. Xu, X. Liu, Q. Li, J. Guo, N. L. Torad, S. M. Alshehri, T. Ahamad, M. S. A. Hossain, Y. V. Kaneti and Y. Yamauchi, *Nanoscale*, 2020, **12**, 15611–15619.
- 23 S. Zhang, W. Xia, Q. Yang, Y. Valentino Kaneti, X. Xu, S. M. Alshehri, T. Ahamad, Md. S. A. Hossain, J. Na, J. Tang and Y. Yamauchi, *Chemical Engineering Journal*, 2020, **396**, 125154.
- 24 D. D. Medina, J. M. Rotter, Y. Hu, M. Dogru, V. Werner, F. Auras, J. T. Markiewicz, P. Knochel and T. Bein, *J. Am. Chem. Soc.*, 2015, **137**, 1016–1019.
- 25 R. P. Bisbey, C. R. DeBlase, B. J. Smith and W. R. Dichtel, *J. Am. Chem. Soc.*, 2016, **138**, 11433–11436.
- 26 Y. Yang, C. Schäfer and K. Börjesson, *Chem*, 2022, **8**, 2217–2227.
- 27 D. D. Bhagwandin, J. H. Dunlap, L. D. Tran, A. Reidell, D. Austin, A. A. Putnam-Neeb, M. Loveday, R. Rao, L. A. Baldwin and N. R. Glavin, *CrystEngComm*, 2024, **26**, 27–31.
- 28 Z. Ou, B. Liang, Z. Liang, F. Tan, X. Dong, L. Gong, P. Zhao, H. Wang, Y. Zou, Y. Xia, X. Chen, W. Liu, H. Qi, U. Kaiser and Z. Zheng, *J. Am. Chem. Soc.*, 2022, **144**, 3233–3241.
- 29 S. Kim and H. C. Choi, *ACS Omega*, 2020, **5**, 948–958.
- 30 Q.-W. Meng, S. Wu, M. Liu, Q. Guo, W. Xian, X. Zuo, S. Wang, H. Yin, S. Ma and Q. Sun, *Sci. Adv.*, 2023, **9**, eadh0207.
- 31 T. Zhang, X. Fu, C. Wu, F. J. Tan, Y. Liu and S. Xia, *Journal of Environmental Chemical Engineering*, 2021, **9**, 106807.
- 32 M. Matsumoto, L. Valentino, G. M. Stiehl, H. B. Balch, A. R. Corcos, F. Wang, D. C. Ralph, B. J. Mariñas and W. R. Dichtel, *Chem*, 2018, **4**, 308–317.
- 33 K. Dey, M. Pal, K. C. Rout, S. Kunjattu H, A. Das, R. Mukherjee, U. K. Kharul and R. Banerjee, *J. Am. Chem. Soc.*, 2017, **139**, 13083–13091.
- 34 A. Kumar Mahato, S. Bag, H. S. Sasmal, K. Dey, I. Giri, M. Linares-Moreau, C. Carbonell, P. Falcaro, E. B. Gowd, R. K. Vijayaraghavan and R. Banerjee, *J. Am. Chem. Soc.*, 2021, **143**, 20916–20926.

- 
- 35 S. A. Ahmed, Q. Liao, Q. Shen, M. M. F. Ashraf Baig, J. Zhou, C. Shi, P. Muhammad, S. Hanif, K. Xi, X. Xia and K. Wang, *Chemistry A European J*, 2020, **26**, 12996–13001.
- 36 D. Zhu, J.-J. Zhang, X. Wu, Q. Yan, F. Liu, Y. Zhu, X. Gao, M. M. Rahman, B. I. Yakobson, P. M. Ajayan and R. Verduzco, *Chem. Sci.*, 2022, **13**, 9655–9667.
- 37 R. L. Li, N. C. Flanders, A. M. Evans, W. Ji, I. Castano, L. X. Chen, N. C. Gianneschi and W. R. Dichtel, *Chem. Sci.*, 2019, **10**, 3796–3801.
- 38 H. Chen, M. Li, Z. Lu, X. Wang, J. Yang, Z. Wang, F. Zhang, C. Gu, W. Zhang, Y. Sun, J. Sun, W. Zhu and X. Guo, *Nat Commun*, 2019, **10**, 3872.
- 39 J. P. Daum, A. Ajnsztajn, S. A. Iyengar, J. Lowenstein, S. Roy, G. Gao, E. H. R. Tsai, P. M. Ajayan and R. Verduzco, *ACS Nano*, 2023, **17**, 21411–21419.
- 40 D. Cui, Y. Fang, O. MacLean, D. F. Perepichka, F. Rosei and S. Clair, *Chem. Commun.*, 2019, **55**, 13586–13589.
- 41 H. S. Sasmal, A. Halder, S. Kunjattu H, K. Dey, A. Nadol, T. G. Ajithkumar, P. Ravindra Bedadur and R. Banerjee, *J. Am. Chem. Soc.*, 2019, **141**, 20371–20379.
- 42 D. D. Medina, V. Werner, F. Auras, R. Tautz, M. Dogru, J. Schuster, S. Linke, M. Döblinger, J. Feldmann, P. Knochel and T. Bein, *ACS Nano*, 2014, **8**, 4042–4052.
- 43 D. Zhu and R. Verduzco, *ACS Appl. Mater. Interfaces*, 2020, **12**, 33121–33127.
- 44 J. W. Colson, A. R. Woll, A. Mukherjee, M. P. Levendorf, E. L. Spitler, V. B. Shields, M. G. Spencer, J. Park and W. R. Dichtel, *Science*, 2011, **332**, 228–231.
- 45 S.-L. Cai, Y.-B. Zhang, A. B. Pun, B. He, J. Yang, F. M. Toma, I. D. Sharp, O. M. Yaghi, J. Fan, S.-R. Zheng, W.-G. Zhang and Y. Liu, *Chem. Sci.*, 2014, **5**, 4693–4700.
- 46 A. M. Evans, A. Giri, V. K. Sangwan, S. Xun, M. Bartnof, C. G. Torres-Castanedo, H. B. Balch, M. S. Rahn, N. P. Bradshaw, E. Vitaku, D. W. Burke, H. Li, M. J. Bedzyk, F. Wang, J.-L. Brédas, J. A. Malen, A. J. H. McGaughey, M. C. Hersam, W. R. Dichtel and P. E. Hopkins, *Nat. Mater.*, 2021, **20**, 1142–1148.

- 
- 47 B. J. Smith, A. C. Overholts, N. Hwang and W. R. Dichtel, *Chem. Commun.*, 2016, **52**, 3690–3693.
- 48 Li, Rebecca L.; Yang, A.; Flanders, N. C.; Yueng, M. T.; Sheppard, D. T.; Dichtel, W. R.; Two Dimensional Covalent Organic Framework Solid Solutions, *J. Am. Chem. Soc.*, 2021, **143**, 7081–7087.
- 49 H. Wang, B. He, F. Liu, C. Stevens, M. A. Brady, S. Cai, C. Wang, T. P. Russell, T.-W. Tan and Y. Liu, *J. Mater. Chem. C*, 2017, **5**, 5090–5095.
- 50 B. Sun, C.-H. Zhu, Y. Liu, C. Wang, L.-J. Wan and D. Wang, *Chem. Mater.*, 2017, **29**, 4367–4374.
- 51 W. Huang, J. Chen, Y. Yao, D. Zheng, X. Ji, L.-W. Feng, D. Moore, N. R. Glavin, M. Xie, Y. Chen, R. M. Pankow, A. Surendran, Z. Wang, Y. Xia, L. Bai, J. Rivnay, J. Ping, X. Guo, Y. Cheng, T. J. Marks and A. Facchetti, *Nature*, 2023, **613**, 496–502.
- 52 Y. Yao, W. Huang, J. Chen, X. Liu, L. Bai, W. Chen, Y. Cheng, J. Ping, T. J. Marks and A. Facchetti, *Advanced Materials*, 2023, **35**, 2209906.
- 53 Q. Fang, Z. Pang, Q. Ai, Y. Liu, T. Zhai, D. Steinbach, G. Gao, Y. Zhu, T. Li and J. Lou, *Proc. Natl. Acad. Sci. U.S.A.*, 2023, **120**, e2208676120.
- 54 P. R. Paudel, J. Tropp, V. Kaphle, J. D. Azoulay and B. Lüssem, *J. Mater. Chem. C*, 2021, **9**, 9761–9790.
- 55 M. Yamashita, C. Otani, H. Okuzaki and M. Shimizu, in *2011 XXXth URSI General Assembly and Scientific Symposium*, IEEE, Istanbul, 2011, pp. 1–4.
- 56 C. M. Proctor, J. Rivnay and G. G. Malliaras, *J Polym Sci B Polym Phys*, 2016, **54**, 1433–1436.
- 57 D. Mullangi, S. Shalini, S. Nandi, B. Choksi and R. Vaidhyanathan, *J. Mater. Chem. A*, 2017, **5**, 8376–8384.

---

58 L. D. Tran, K. F. Presley, J. K. Streit, J. Carpena-Núñez, L. K. Beagle, T. A. Grusenmeyer, M. J. Dalton, R. A. Vaia, L. F. Drummy, N. R. Glavin and L. A. Baldwin, *Chem. Mater.*, 2022, **34**, 529–536.